Continental Shelf Research 44 (2012) 30–38

Contents lists available at SciVerse ScienceDirect

Continental Shelf Research

journal homepage: www.elsevier.com/locate/csr

Research papers

Tracking bottom waters in the Southern Adriatic Sea applying seismic oceanography techniques

Sandro Carniel [a,*], Andrea Bergamasco [a], Jeffrey W. Book [b], Richard W. Hobbs [c], Mauro Sclavo [a], Warren T. Wood [b]

[a] C.N.R.—Institute of Marine Sciences, Venice, Italy
[b] US Naval Research Laboratory, USA
[c] Department of Earth Sciences, University of Durham, UK

ARTICLE INFO

Article history:
Received 28 April 2011
Received in revised form
6 August 2011
Accepted 15 September 2011
Available online 5 October 2011

Keywords:
Seismic oceanography
Reflectivity
Thermohaline structures
Southern Adriatic Sea

ABSTRACT

We present the first results from the seismic oceanography (SO) cruise ADRIASEISMIC where we successfully imaged thermohaline fine structures in the shallow water environment (50–150 m) of the southern Adriatic Sea during March 2009 using a compact two GI-gun seismic source. The SO observations are complemented with traditional oceanographic and micro-structure measurements and show that SO can operate over almost the entire water column except (in our experimental layout) for the uppermost 50 m. After processing to enhance the signal-to-noise ratio, the seismic reflection data have a vertical resolution of ~10 m and a horizontal resolution of ~100 m and provide a laterally continuous map of significant thermohaline boundaries that cannot be achieved with conventional physical oceanography measurements alone. ADRIASEISMIC specifically targeted structures in shallow waters, namely along the western margin of the southern Adriatic Sea, between the Gargano peninsula and the Bari canyon, and imaged the Northern Adriatic Dense Water (NAdDW), a bounded cold and relatively dense water mass flowing from the northern Adriatic Sea.

The seismic data acquired in Bari canyon and offshore of the Gargano promontory show many regions of strongly reflecting shallow structures, and the incorporation of XBTs measurements with these data demonstrate that they can be interpreted in terms of temperature structures and gradients. In the Gargano region several warm water intrusive structures are mapped along with the offshore transitional edge of cold waters of strong NAdDW influence. In Bari Canyon, waters with NAdDW influence are further mapped extending over the shelf and off the slope into a 5 km long tongue extending offshore between depths of 200 and 300 m. More generally, even though neither cascading nor open-ocean deep convection process appeared to be evident during March 2009, the SO approach was able to map details of thermal features not resolved by even closely spaced XBT measurements.

1. Introduction

Using the techniques primarily designed to map sub-seafloor geologic structures, a new discipline called Seismic Oceanography (SO) was recently shown to be capable of providing images of water layers in the ocean (Gonella and Michon, 1988; Holbrook et al., 2003; Papenberg et al., 2010).

The lower frequency sound waves used in SO (from 10 to 200 Hz) are coherently reflected directly by the thermohaline boundaries between water masses on the scale of meters to tens of meters (Ruddick et al., 2009).

This coupled with hydrophone spacing of 12.5–25 m means that the seismic oceanographic records can provide measurements of the structure of the ocean water masses with resolutions of the order of 6–12 m both horizontally and vertically (Hobbs et al., 2009; Geli et al., 2009) which, when compared to typical oceanographic eXpendable Bathy-Thermographs (XBTs) or conductivity-temperature-depth (CTD) casts with a spacing of 1–10 km, is an increase of several orders of magnitude in horizontal resolution. This approach represents therefore a new possible way of observing transient small scale ocean phenomena characterized by high time–frequency.

The generation of the seismic images is challenging as the reflections from thermohaline boundaries in the ocean are about 1000 times weaker than those from sediment interfaces, and in order to show subtle details in the water masses the reflections require careful processing of high quality seismic data.

Moreover, although seismic reflections from water mass boundaries have been reported and several analyses performed using combined seismic and XBT data (Holbrook et al., 2003;

* Corresponding author. Tel.: +39 329 0845720.
E-mail address: sandro.carniel@ismar.cnr.it (S. Carniel).

0278-4343/$ - see front matter © 2011 Elsevier Ltd. All rights reserved.
doi:10.1016/j.csr.2011.09.004

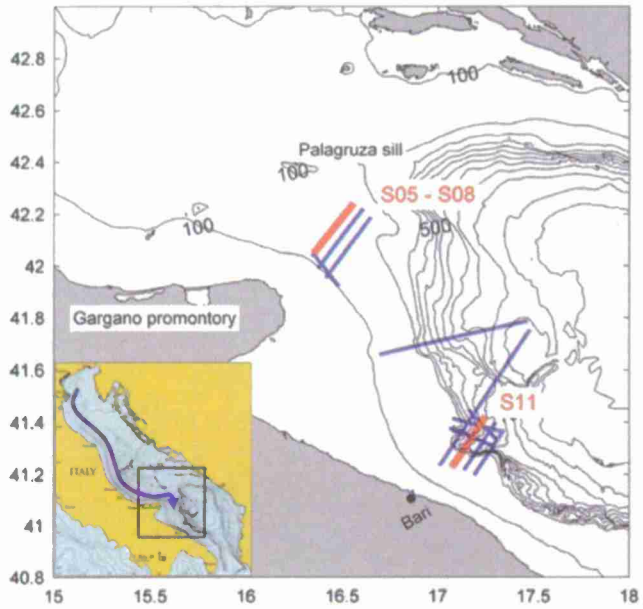

Fig. 1. Bathymetry of the investigated region with highlighted all the seismic lines occupied during the ADRIASEISMIC cruise (light blue, thin lines). Bold red lines are those presented in this paper. Total number of successfully acquired lines (some of them occupied more than once) was 17. The blue arrow from N to S denote the general path followed by the NAdDW. (For interpretation of the references to color in this figure legend, the reader is referred to the web version of this article.)

Nandi et al., 2004; Wood et al., 2008), dedicated SO field programs including full seismic *and* oceanographic measurements have only been performed in the Kuroshio Extension in the Western Pacific (Nakamura et al., 2006; Tsuji et al., 2005), in the Mediterranean outflow area of the Eastern Atlantic (Hobbs et al., 2007; Papenberg et al., 2010) and in the Gulf Stream system (Mirshak et al., 2010). In these cases, the water column objectives were large-scale features in water greater than 200 m deep.

This paper describes preliminary results from the international ADRIASEISMIC cruise (March 3–16, 2009) carried out on board the CNR R/V *Urania* in the southern Adriatic Sea. It was the first SO experiment that (i) specifically targeted structures in shallow waters (along the western margin of the Adriatic Sea between the Gargano promontory and the Bari canyon, see Fig. 1) and (ii) devoted particular attention to a tight integration of other physical oceanography measurements with the seismic reflection images of water structure (namely, besides classical CTDs and XBTs deployment, also acquired Lowered Acoustic Doppler Current Profiler (LADCP) data and 101 turbulence micro-structure casts). Further details can be found by Wood et al. (2011).

Together, the direct oceanographic sampling provided a full range of vertical resolutions down to the micro-structure scale to complement the high lateral resolution of the seismic image.

The paper is organized as follows: after a short Introduction, Section 2 briefly discusses the Materials and Methods employed, then Section 3 outlines the Southern Adriatic Sea dominant features, while Section 4 presents some preliminary results along a selection of different sections. Eventually, in Section 5 some suggestions and recommendations are given.

2. Materials and methods

During the ADRIASEISMIC campaign we employed the SO technique to identify the different water masses present along the central/south Adriatic slope and to detect the North Adriatic Dense Water (NAdDW) flowing southward from the coastal shelf (see Fig. 1). into the deeper basin. As better explained in Section 3, this is a complex process as the cold and fresh bottom water flows along the shelf and descends through local canyon systems, encountering and mixing with ambient warmer and saltier water, usually resident in the deep basin (Vilibic and Supic, 2005).

The temperature contrasts and the relatively small spatial scales that characterize these processes were thought to be well suited for testing the SO technique in shallow waters. Previous SO cruises have typically used significantly larger sources and receiver arrays requiring the use of larger and more specialized vessels. We used a compact seismic system that could be deployed quickly off a medium-sized (61 m) research vessel, using only two small air-guns and a 1.2 km hydrophone receiver array for greater flexibility in switching modes between seismic and conventional physical oceanography measurements, in order to allow for adaptive sampling of these quickly evolving shelf and coastal processes.

Since SO measurements alone are not sufficient, at least at this present stage, to fully characterize such complex processes, the resulting seismic reflection data had to be combined with a series of more "classical" physical oceanography measurements, such as traditional CTDs, LADCP measurements of ocean currents and 232 XBT casts simultaneous with SO sections. In addition to this, micro-structure measurements (allowing a very high resolution via a free-falling profiler, for a total of 101 casts) were for the first time acquired together with the seismic measurements, providing data on a full suite of important oceanographic variables at high vertical resolutions, which are useful in determining the connections between SO measured vertical temperature changes and small-scale dynamical factors (Carniel et al., 2010; Wood et al., 2011).

A sketch of the acquisition geometry for ADRIASEISMIC is shown in Fig. 2. A ship moving at ~4 knots tows a controlled sound source and a linear array of hydrophones, both at a depth of a few meters. The sound source is typically an air-gun, a device that explosively releases compressed air, creating a sound pulse in the ocean with a duration of 5–10 ms. A small fraction of the sound pulse reflects off of near-horizontal interfaces such as sediment layers in the earth or temperature/salinity changes in the ocean, and the reflected energy is then recorded at the hydrophone array, also towed by the ship. Typically, the source is fired every 25 m (about every 12 s). The hydrophone array

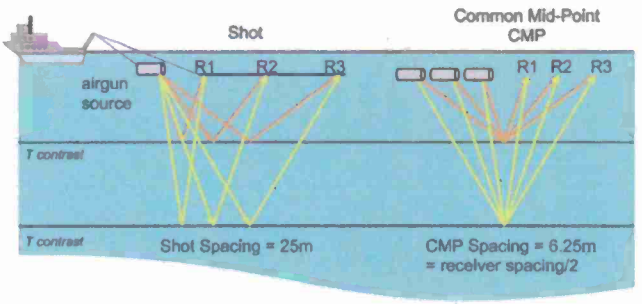

Fig. 2. Seismic data are acquired while towing a source, and a receiving array. During ADRIASEISMIC we used an array of one or two generator–injector air guns for the source, and a 1200 m, 96-channel hydrophone array for the receiver. Each channel consisted of 16 individual hydrophones whose signals were summed in real time to produce a single record of pressure vs. time. Individual source–receiver records were rearranged post-acquisition into common mid-point (CMP) bins such that reflection points coincide. Time differences were removed (normal move-out correction) and CMP records summed to enhance the signal to noise ratio.

contains groups of 10–20 closely spaced individual hydrophones that are summed to generate a single channel record with a horizontal spacing of 12.5 m. An array may contain tens to hundreds of channels, with each one providing an independent measurement of ocean reflectivity for each firing of the source. For our survey the source used one or two generator-injector airguns and a 1.2 km receiver array containing 96 channels.

The backscattered sound, seismically measured by the array, is the signal S, a convolution between the acoustic wavelet (W) of the sound source and the water column reflectivity R:

$$S = W * R = W * \frac{I(z_-) - I(z_+)}{I(z_-) + I(z_+)} \quad (1)$$

The water column reflectivity is created by changes in the acoustic impedance $I(z)$ at a contact between two water masses, defined as the product of $\rho(z)$, the *in situ* water density, and $c(z)$, the sound speed, both of which are a function of temperature, salinity and depth. Here we use the oceanographic convention of z pointing upwards, but also maintain the seismic convention of an increase in impedance downward (e.g. cold water over warm) producing a positive seismic reflectivity. The water column profile of the dimensionless reflection coefficient, R in Eq. (1), closely resembles the profile of dT/dz, once it is scaled adequately (Ruddick et al., 2009). Even though variations occur among different water masses, Sallarès et al. (2009) found that about 80% of the reflectivity variations in the oceans are due to temperature gradients.

Processed seismic data does not record the long wavelength (> 30 m) gradational change in water properties from the surface to the seabed, and can only recover the short (0–20 m) wavelength changes at discrete thermohaline boundaries (Papenberg et al., 2010). A high frequency signal (> 100 Hz) offers a high vertical resolution and can detect boundaries with a 5 m separation (Geli et al., 2009) but may be unable to detect a smooth temperature (salinity) gradient over 25 m between two water masses. Lower frequency signals (< 20 Hz) will detect these boundaries, but will not be able to resolve the finer scale boundaries and will give an integrated response (Hobbs et al., 2009). It is therefore important to design the acquisition layout to produce the best frequency range for the anticipated target and then use appropriate processing filters to produce the final data. Equally it is important to interpret the final processed data with understanding of these issues in order to better analyze different interfaces and layers thickness. Hobbs et al. (2009) showed that large impedance contrasts covering several tens of meters vertically are best observed using a low frequency source (~20 Hz), whereas higher frequencies are more suited to viewing finer structures. Hence, information regarding the thickness of the layer and the gradient intensity of the interface may be related to the clarity of the observed reflections in the seismic image.

The vertical resolution of a seismic section is between 1/4 and 1/8 of the dominant wavelength (Sheriff and Geldart, 1995). The two GI-gun source array used for 13 of the 17 lines of this survey was operated in "harmonic mode" (Landrø, 1992) and produces a broadband acoustic impulse which, when convolved with the free-surface reflection, produces a far-field wavelet with a spectrum largely controlled by the source tow-depth of 3 m. The average frequency spectrum for the processed data (see Fig. 3) shows the −6 dB bandwidth of about 38–80 Hz. This gives a minimum wavelength of about 20 m, i.e. a vertical resolution of 2.5–5 m, assuming a sound speed of 1509 m/s. Therefore the seismic frequency used is particularly suited to resolve boundaries ~10 m. However, it is important to bear in mind that each seismic data point draws significantly from a 30–40 m length

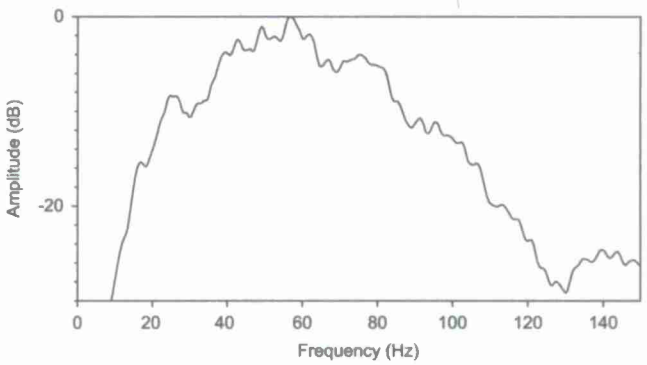

Fig. 3. Amplitude spectrum of the processed seismic data. Note the notch at 125–130 Hz caused by the free-surface reflection at the 6 m depth source array and the peak response from 38 to 80 Hz (points greater than −6 dB level).

vertical bin of water column reflectivity (see Eq. (1)) through the wavelet convolution.

For the processed seismic data presented here, the highest horizontal resolution is equal to the width of Fresnel zone whose radius, R_f, varies with depth z and seismic frequency f according to the approximate formula $R_f = (Vz/2f)^{1/2}$ where V is the sound speed (Sheriff, 1980), which gives, for a target depth of 100 m, a Fresnel zone diameter of ~75 m. Note that this distance corresponds to the ability to completely resolve reflectors; changes in the reflection amplitude and phase can be detected over much shorter distances. However, for the final image, the horizontal resolution is limited to about 90 m since, in order to increase the signal to noise ratio, a lateral mix of 7 traces, spaced every 12.5 m, is applied. This boost to the signal to noise ratio is critical to make the coherent reflections visible above the ambient noise and is a tradeoff with the signal to noise during data acquisition. The airgun source-size and shooting interval is determined by the capacity of the compressor to supply the necessary high-pressure air, the minimum ship's speed required to control the receiver array, the surface currents and the good practice to have a serviceable spare to minimize repair time, should one of the guns fail. Though a larger volume source, e.g. a three GI-gun array, would have improved the signal to noise on the raw data, the corresponding increased shot spacing would have reduced the number of raw traces in the processing with a negative effect on the quality of the final seismic reflection section. During the cruise a number of different source configurations were tried and the two gun solution proved to be best given the resources at hand, and therefore was used most often. However, a single gun firing in true GI mode was used for four of the sections and this also produced adequate seismic oceanography data.

The objective of the processing applied to the seismic data is to enhance the required reflected energy against the other signal (noise) sources. The processing steps are listed in Table 1 and we discuss the critical steps here. After fixing the geometry and a bandpass filter to suppress low-frequency surface wave and tow noise and energy above 200 Hz, a median filter is used to suppress direct wave. The relatively high-energy wave propagates horizontally from the source to the receiver array and may interfere with the required reflected energy. The data are then sorted to common-mid-point (CMP) gathers so each CMP contains traces with various source–receiver offsets where the reflections have come from the same sub-surface point assuming a locally 1-D structure. Prior to stacking the traces in each CMP gather, they need to be corrected for the offset dependency though a process call normal move-out (Dix, 1955), this requires knowledge of the sound speed structure of the water, which was derived from the XBT casts with salinity inferred from CTD data.

Table 1
Processing steps used to convert the raw seismic data into the sections used in the paper.

Processing sequence number	Process name	Description
1	Geometry	Fix the locations of the shots and receivers for each trace knowing the location of the vessel and receiver array from GPS and compass measurements
2	Minimum-phase bandpass filter	Suppress seismic noise outside the seismic signal bandwidth that includes surface wave and tow noise
3	Median filter	Suppress the direct wave energy that has not undergone a reflection
4	Sort to CMP gathers	Based on the geometry (#1) collect together all traces that have a common mid-point which, for a local 1-D model, is equivalent to traces with the same sub-surface reflection point
5	Normal move-out	Apply a sound speed dependent geometrical correction to correct for the various source–receiver offsets within each CMP gather. The sound speed model is derived from the coincident XBT casts
6	Stack	Sum all the traces within each CMP gather to form a single stack trace at the location of the CMP, which when displayed side-by-side form a seismic profile
7	Static shift	Correct for known delays in acquisition system and minimum-phase filter (#2)
8	Mixing	A lateral running mix to increase the signal to noise ratio of the data
9	Display	Apply a gain to the profile so the weak thermohaline reflections can be visualized

3. The Adriatic context

The general circulation of the Adriatic Sea is characterized by having an almost permanent feature known as the Western Adriatic Current (WAC). It is the branch of a basin cyclonic flow that carries along the Italian coast both surface water masses (usually heavily affected by the Po river, the largest of the whole basin) and deeper, denser ones (Vilibic and Supic, 2005). The latter may form during winter time on the broad, shallow shelf in the north Adriatic basin exposed to the Bora winds bringing cold, dry air from the north-east down the Dinaric Alps (Dorman et al., 2006). Indeed, the resulting intense evaporation and cooling of the shelf waters may produce North Adriatic Dense Water (NAdDW), which then tends to sink and "cascade" all the way to the southern basin. During these rather episodic formation processes, more frequent during winter time (Bergamasco et al., 1999), the main controlling factors are intense cold wind outbreaks, the ambient water density, preconditioned during late autumn, and also other factors, e.g. river discharges. When such processes of buoyancy extraction happen, several isopycnic surfaces outcrop and very often the whole water column (20–25 m deep) may be ventilated. However, the general process of northern water masses flowing to the southern part of the Adriatic basin is complex and far from being completely understood.

While flowing southward, the water masses may get diluted and/or affected by entrainment of ambient water masses (which in turn can change the dynamical constraints and modify the trajectory and the buoyancy), until reaching their neutral density level or filling topographic depressions and then overflowing. Typically these bottom waters become topographically adjusted around 80–120 m depth and form a relatively narrow stream (a few kilometers wide and some tens of meters thick) that flow southward on the western margin of the Adriatic Sea. These narrow streams are considered important, since the fate of these relatively dense waters may affect the whole basin circulation and is most likely involved in triggering sediment flux processes (Turchetto et al., 2007). Unfortunately, they are difficult to observe and detect by conventional oceanographic approaches such as CTDs sampling, because of their small horizontal scale.

Moreover, once in the central-southern Adriatic area, currents can produce eddies and filaments, e.g. in proximity of the Gargano area (Burrage et al., 2009), and the cold and fresh water may sink and mix with saltier and warmer surrounding waters. The Gargano frontal region is indeed known to be very active and characterized by a hyperbolic flow point (see Taillandier et al., 2008), where different water masses of compensating densities, intrusions and interleaving structures can create complex mixing situations (Carniel et al., 2008).

In addition to the above described formation mechanism, which is mainly a shelf process, open ocean deep convection processes may also produce local dense water masses, albeit limited to the southern part of the Adriatic Sea and mostly during winter. These processes have been described and observed in a relatively deep region (see Vilibic and Supic, 2005) but they can also possibly interact with the NAdDW flow.

Manca et al. (2002), using CTD data collected in 1998–1999, could detect both open-ocean convection down to intermediate depths and lateral advection of dense water from shallow shelf zones, indicating the importance of the NAdDW in filling up the South Adriatic dense water reservoir. Once in the proximity of the Bari canyon region, the interactions with the steep topography can break the potential vorticity constraint, increasing the descent velocity to the South Adriatic Pit. A more complete discussion of these features, including hypotheses about the most common paths taken by these dense water veins, can be found in Vilibic and Supic (2005).

Fig. 1 shows our area of investigations and the section lines where SO and simultaneous XBTs were deployed during the ADRIASEISMIC cruise. In total, 17 lines were successfully collected and analyzed. For brevity, here we will concentrate only on a restricted number of examples that best illustrate the processes of dense water descent.

4. First results

During the cruise, in the area facing the Gargano promontory several seismic lines perpendicular to the coast were carried out and complemented with XBT, CTD casts, LADCP and microstructure measurements.

Seismic data were acquired more than once along each of the three lines perpendicular to the coast near the Gargano promontory, in order to examine the time evolution of the seismically observed structures.

As preliminary results, we firstly analyze the lines S05 and S08 (Fig. 4) off the Gargano promontory (see Fig. 1), which are two of the lines acquired in this area where it could be expected to track the "last" coastal part of the descending vein of the NAdDW flowing southward, before its interaction with the steep topography at the Bari Canyon.

We will here focus on the intermediate-depth reflectivity signals, mostly below 50 m. The yellow and darkest blue areas denote regions with the strongest vertical temperature gradients, though the bottom yellow/red stripe is most likely an artefact caused by the high reflection coefficient in the adjacent seabed.

It is useful to note that due to the wavelet, an isolated water column reflectivity feature will in general produce a series of positive and negative bands in the seismic image. For our setup,

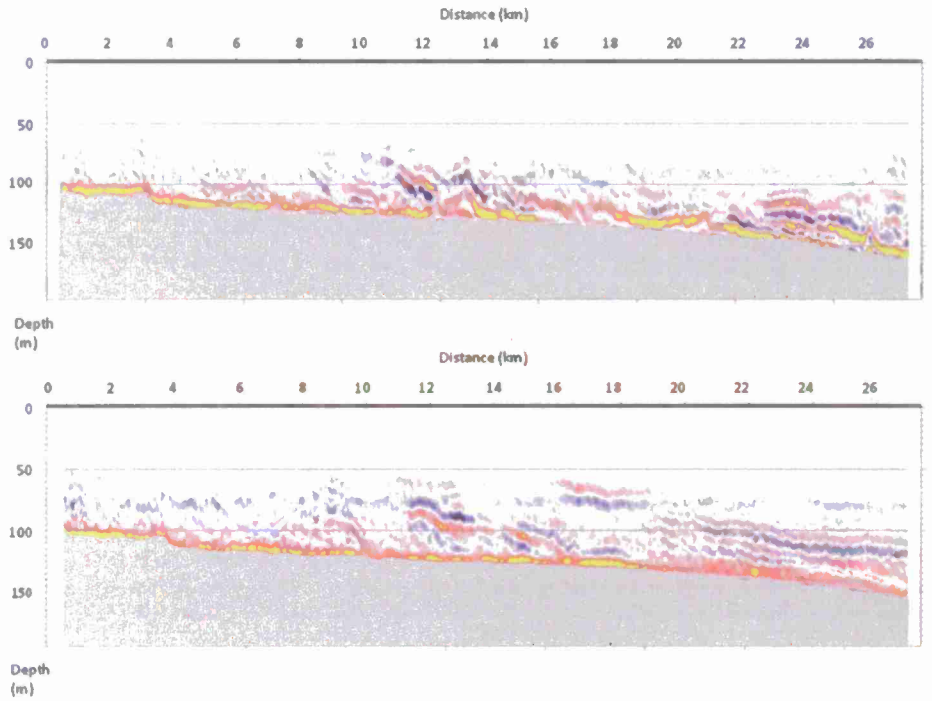

Fig. 4. Seismic data acquired along the S05 (upper panel) and S08 (lower panel) lines. Both lines occupied the Gargano region and were taken in the inshore–offshore direction (see Fig. 1). The S05 section was obtained using two GI guns operated in harmonic mode and the S08 section was obtained using a single GI gun operated in true GI mode. Blue/black are positive signals and red/yellow are negative signals (see Eq. (1)). The color scales are relative to each survey due to differing acquisition setups. (For interpretation of the references to color in this figure legend, the reader is referred to the web version of this article.)

the strongest pair of the sequence from a positive reflectivity feature is a negative over a positive band, and therefore an isolated red over blue band is a cold over warm feature. The exact sequence in the reflection bands is determined by the combination of data acquisition and processing and, for any seismic section, best calibrated using a known impedance boundary like the seabed. Also if water column interfaces are closer together to each other than 30–40 m in the vertical, than the resulting superimposed band pattern will of course be more complicated.

Both lines were performed in the direction offshore–inshore, in two different periods: the former was performed on March 9th, from 11:31 to 15:16 UTC, while the latter was acquired on March 11th, from 08:13 to 11:58 UTC. Thus they provide a view of the same region about 45 h apart, before and after a storm passed through the area with intense Sirocco winds from the south. Some of the features depicted by the reflectivity values change between the two surveys (see Fig. 4), but there seem to be also some qualitatively consistent aspects in both passes as well.

For example, in the section bracketed by 11–16 km, both figures present a strong reflectivity region where the signals, although differing in some details, show a general downward slope from about 75 m depth to the bottom. Further offshore, both lines again present strong reflection signals, but of different structures. A doming structure appears around 23 km near the bottom of line S05, and a slightly weaker reflecting structure, more parallel to the bottom, is evident in line S08 at 19–27 km.

Generally speaking, therefore, while these figures provide us with a striking direct estimate of the scales of structures observed, they do not always elucidate their nature.

To complete the oceanographic view and help interpret these results, we need to integrate them with the temperature sections obtained from the coincident XBT casts. All XBT data were processed with the standard manufacturer depth conversions.

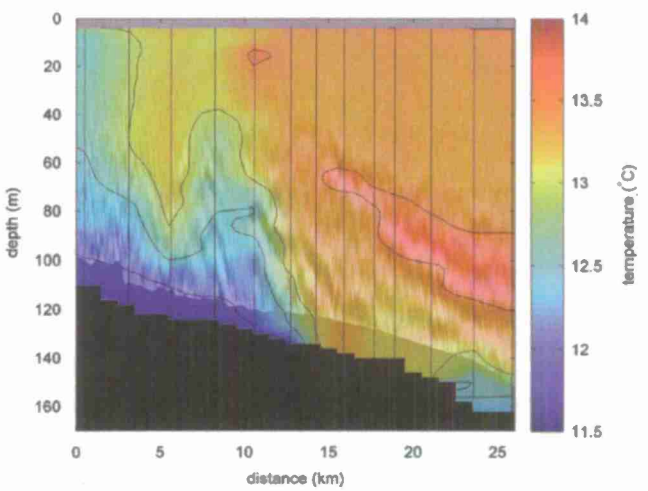

Fig. 5. Processing of seismic data acquired along line S08, with the estimated temperature field superimposed in semi-transparent color over the seismic image in grayscale. The seismic data points are plotted according to the depth in their bin where the first trough of the wavelet interacts with the water column reflectivity. The position of each XBT cast is shown by a vertical black line, and the temperature field was reconstructed by means of a kriging technique. Contours (curving black lines) are drawn every 0.5 °C. The zone of overlap at the bottom is mainly due to a mask applied to the seismic data to eliminate potential near-bottom artefacts. (For interpretation of the references to color in this figure legend, the reader is referred to the web version of this article.)

As an example, Fig. 5 shows the same seismic image presented in Fig. 4 (line S08, lower panel), with now the estimated temperature field superimposed in color over the seismic image in grayscale. The temperatures were obtained by interpolating the temperature measurements registered by 13 of the XBTs launched along the line. Only T-5 types were used for this due

to our observation that they had better depth accuracy than T-11 types under the manufactured depth conversions. The position of each XBT cast is shown by a vertical black line, and the field was reconstructed by means of a kriging technique. Contours (curving black lines) are drawn every 0.5 °C.

There is a generally good qualitative agreement between the temperature field reconstructed from the XBTs launched during the line and the reflectivity signals. The horizontal structure of the bottom part of the warm water intrusion (15–26 km) is particularly well captured by the seismic technique, as can be seen by the dark/light/dark structure that tracks the 13.5 °C isotherm line. This overlay also enables the interpretation of the features seen in the seismic image, e.g. the strong dark reflector from 10 to 13 km can be related to the upper boundary of a warm tongue (note the hook in the 12.5 °C isotherm) penetrating into the top of NAdDW influenced waters. Note how the seismic image can show a much greater detail of this feature with respect to that captured by the two XBTs spanning it in the figure. Of course, the XBT interpolated field is not expected to perfectly match the seismic images; it is indeed in these cases, especially in frontal regions, that the benefit of the SO approach should be superior to that of a "classic" oceanographic mapping, even with the XBT cast spacing of 2 km used here, which is much closer spaced than in a typical survey. Also, interpolation of XBTs can lead to some artefacts, which are particularly evident in the regions where the casts are less dense (e.g. around 3–6 km) or where the seismic image shows that the structure of features are changing rapidly over short spatial scales (e.g. around 9–11 km). It appears therefore evident how seismic records, once adequately scaled with regards to the temperature field, could possibly be used to interpolate between vertical profiles, providing a significant increase of detail of resolution.

Fig. 6 presents an enlarged portion of Fig. 5 (bracketing the region between 6 and 10 km, which was covered by XBT 124) showing (from left to right): the XBT measured temperature profiles (°C) (panel "a"), the XBT temperature gradient dT/dz calculated from the profiles (panel "b"), and the corresponding seismic data (panel "c").

This enlarged picture shows that the strong seismic signals seen near 8 km are related to temperature undulations in the transition of water column temperature from 12.75 °C at 60 m to the 11.9 °C of NAdDW core water found at the bottom. The blue peak in the seismic image at 100 m aligns with a positive peak in dT/dz, and the sharp downward slope of the reflectors towards offshore suggests that the NAdDW boundary thickness is decreasing here. This generally agrees with a thinning of the NAdDW core as observed by the XBTs (see Fig. 5).

If we consider again Fig. 4, we can state now that the strong reflectivity signals in the 11–16 km region detected in lines S05 and S08 are associated with the offshore transitional edge of the colder NAdDW core and waters of NAdDW influence. We find that the area of the region of influence is not very large and the temperatures in the core are not as cold as typical NAdDW. Book et al. (2010) suggest that the 2009 winter pre-conditioning was not favorable to the formation of a sufficient amount of NAdDW, and as a consequence a less intense signal of these dense waters characterized the regions of study during ADRIASEISMIC. One of the possible reasons for this can be ascribed to the climatic conditions of the northern Adriatic during winter–spring 2009. Indeed, despite the relatively severe winter conditions, the spring was characterized by large fresh water discharges of the rivers on the western Adriatic coast (Book et al., 2010), which contributed to the production of less dense water pools in the source area.

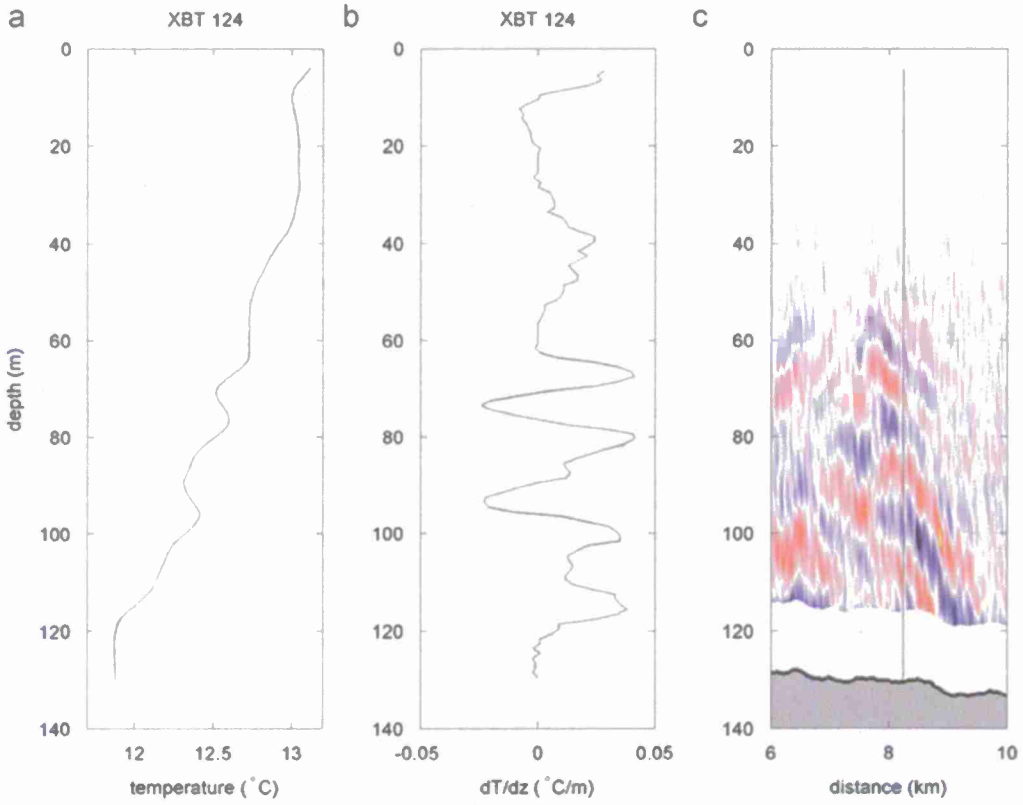

Fig. 6. As in Fig. 5, but showing separately (from left to right): an XBT measured temperature profiles (°C, panel "a"), the XBT temperature gradient dT/dz calculated from the profile (°C/m, panel "b"), and the corresponding seismic data (panel "c") bracketing the region between 6 and 10 km that was covered by this XBT. A zone at the bottom of panel c has been masked in white to eliminate potential near-bottom artefacts.

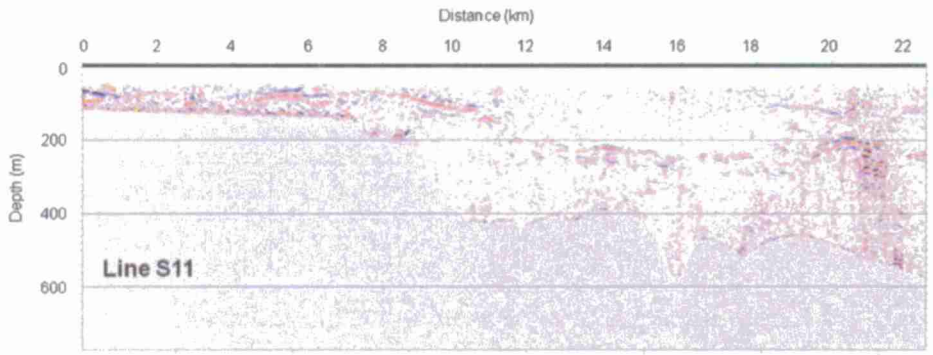

Fig. 7. As in Fig. 4, but for seismic data acquired along the S11 line, cutting through the BCS, inshore–offshore direction. The S11 section was obtained using a single GI gun operated in true GI mode.

This is also partially supported by other data (Cardin et al., 2011). Nevertheless, the fact that we could detect and capture this relatively weak signal represents an indication of the potential of SO, which may be even better exploited during less challenging (in terms of dense water amounts) circumstances. SO was used successfully to map a dense water cascade over the deep Wyville-Thomson Ridge to the north-west of Britain (Polton et al., 2011) using commercial data. As is typically the case when using commercial seismic data, their study was limited by a lack of calibrating XBTs simultaneous with seismic measurements, but it does provide another example of SO's potential application to research such processes.

A further example of acquisition along line S11 is shown in Fig. 7, acquired on March 13th from 19:17 to 22:51 UTC and cutting through the Bari Canyon System (BCS), in an inshore to offshore direction. Interest in this region was motivated also by the observations presented by Turchetto et al. (2007), that during the spring, a vein along the Adriatic shelf of NAdDW was associated with high particle fluxes down the canyon.

There are several areas of significant reflectivity in the S11 seismic image, most notably over the shelf around 4–7 km, dipping off the shelf around 8–10 km, and at depths greater than 200 m offshore, e.g. around 13–16 km. Farther offshore (21 km) there is also a strong reflectivity observed between 200 and 400 m with a suggestion of a slight doming structure.

Fig. 8 presents the same seismic image presented in Fig. 7 (line S11) with the reconstructed temperature field made by a kriging technique of the XBT measurements along the line, superimposed. (Please note that the temperature field and temperature contours are constrained by an additional XBT acquired further offshore that is not displayed). Two T-11 XBTs were used along with the T-5s for this section due to the relatively sparser coverage compared to the S08 line. Contours (thin black lines) are drawn every 0.2 °C, and the temperature color scale spans only from 13 to 14 °C, as opposed to the larger scale used for Fig. 5.

In Fig. 8 there is a mass of water less than 13.3 °C occupying the bottom of the shelf and the slope of the canyon. From this water mass, a relatively narrow tongue of colder water extends offshore for more than 5 km in the depth range of 200–300 m. This water is modified from the NAdDW influenced waters observed off the Gargano promontory, having been diluted and mixed with ambient waters. A nearby CTD line (not shown) done after the seismic survey shows that these cold waters lie on the isopycnal mixing line between NAdDW and modified Levantine Intermediate Water (~13.9 °C, 38.8), and establishes the NAdDW influence in Bari Canyon during our survey.

The reflections from the top of this water mass and the top of the offshore extending tongue are visible in the seismic image. The seismic reflections also imply that there may be a connection

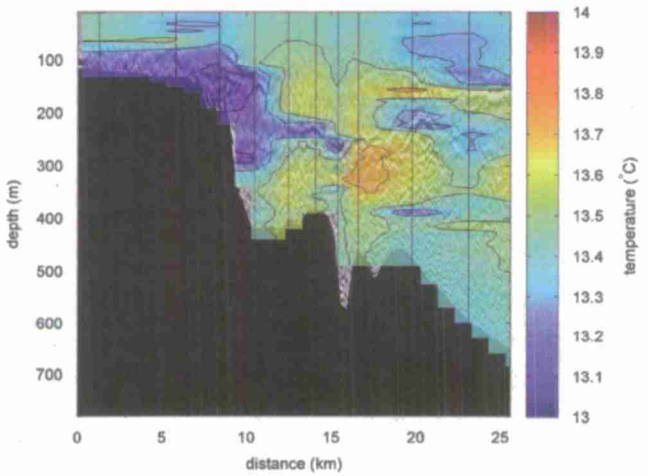

Fig. 8. As in Fig. 5, the estimated temperature field superimposed in semi-transparent color over the seismic image, but for the seismic data acquired along line S11 (see Fig. 7). Contours are drawn every 0.2 °C, at 13.1, 13.3, 13.5 and 13.7 °C. The color scale has been adjusted to better match the temperatures observed along this line. (For interpretation of the references to color in this figure legend, the reader is referred to the web version of this article.)

between the cold tongue and a larger mass of cold water in the same depth range located farther offshore (17–25 km). I.e. the upper boundary of the 200 m deep water mass at 20 km is mapped by a reflector in the seismic image that connects to the XBT observed tip of the cold tongue at 17 km, although the krigged temperature field does not connect them. This is another possible example of the SO technique capturing a feature that would be missed by even closely spaced conventional hydrographic surveys. However, neither cascading to the bottom of the canyon nor open-ocean deep convection processes are evident in the XBT or seismic datasets.

5. Final considerations and recommendations

The seismic measurements collected during ADRIASEISMIC cruise allowed us to demonstrate that SO can operate and map oceanographic features in shallow regions characterized by complex water mass structures, where usually very high-resolution sampling is required. Even XBTs as close together as 2 km lack the horizontal detail and spatial connections that are evident from SO measurements.

SO is particularly well suited for the study of the dynamics of bottom-trapped water masses as compared to classic

techniques: it measures the full water column at ~10–100 m horizontal resolution, depending on the data acquisition and necessary processing to make the reflections visible; it measures remotely and measurements are not hampered by a sloping bottom or concerns of instrument bottom impact, and it can operate successfully over the entire range from 100 m to 1000 m bottom depths for tracking water-mass evolution down a slope (shown for the first time in this cruise).

In addition to this, the high quality ADRIASEISMIC data set demonstrates that SO can be carried out from oceanographic vessels of medium size using a small portable seismic system. The ability to conduct this research without the need for a specialized vessel is a significant step as it opens up the potential of using this novel method to map targets like these important dense water flows.

SO is now at a turning point in its development. Several authors have demonstrated that high resolution seismic observations are possible, but some aspects of the future development of the technique will likely determine if it will be incorporated as a practical standard research or operational oceanographic tool. Important aspects and considerations include the development of optimal field parameters, the ease of use, and the development of signal processing.

Field parameters such as source strength, streamer length, etc. will affect the ease of deployment, weather windows, quality of the data, and the level at which SO and more familiar physical oceanography measurements might interfere with each other (e.g. Geli et al., 2009).

Also, SO records are different from existing oceanographic records and significant algorithm development (e.g. Holbrook and Fer, 2005; Pàramo and Holbrook, 2005; Wood et al., 2008; Papenberg et al., 2010) is required to optimally incorporate them with CTDs, sea surface temperature measurements from satellites, turbulence measurements, etc. Although some important achievements have been made in qualitatively interpreting SO data, the full potential to use this new view of the ocean's thermal structures to quantitatively address questions on the ocean dynamics has yet to be realized.

Last but not least, a careful cost vs. benefit analysis has to be performed. The cost for *renting* a seismic system is comparable with that of *buying* other oceanographic systems like a Scanfish, an Underway CTD, or a micro-structure probe; generally seismic oceanography investigations are more expensive for oceanographers, unless a group already owns its own seismic acquisition system. The potential benefit has to be evaluated case by case, while for some particular applications a ~10 m horizontal resolution measurement related to dT/dz may be highly desirable or essential, in other circumstances a lower resolution measurement, which might include other desirable oceanographic parameters obtained with cheaper systems having comparable speed of acquisition, may be enough.

The experience of ADRIASEISMIC is valuable to evaluate all these issues, since for the first time it provided an example of SO applied to coastal seas where all applicable ocean variables were sampled at very high resolution together with seismic images, allowing us to explore some of the limits and capabilities of seismic methods for characterizing various ocean processes.

Acknowledgements

The authors gratefully acknowledge the Master and crew of the R/V *Urania* (Italian National Research Council, CNR), the seismic acquisition of G. Bortoluzzi (CNR-ISMAR Bologna) and Exploration Electronics LTD and the assistance of K. Schroeder and M. Borghini (CNR-ISMAR La Spezia) in the XBTs analysis. The seismic data were processed at NRL and also by E. Midgley (University of Durham, UK) using Seismic Unix processing software and the Landmark Promax software provided under their University Grants Scheme. Partial support for this work was provided by the Office of Naval Research under Program Element 0601153N. The work was supported by the FIRB Project "DECALOGO", code RBFR08D828_001 by the Italian MIUR.

References

Bergamasco, A., Oguz, T., Malanotte Rizzoli, P., 1999. Modeling dense water mass formation and winter circulation in the Northern and Central Adriatic Sea. Journal of Marine Systems 20 (1–4), 279–300.

Book, et al., 2010. A comparison study of North Adriatic Dense Water descent using observations in March 2006 and March 2009. Geophysical Research Abstracts, EGU General Assembly 12 EGU2010-7766-2.

Burrage, D.M., Book, J.W., Martin, P.J., 2009. Eddies and filaments of the Western Adriatic Current near Cape Gargano: analysis and prediction. Journal of Marine Systems 78, S205–S226. doi:10.1016/j.jmarsys.2009.01.024.

Cardin, V., Bensi, M., Pacciaroni, M., 2011. Variability of water mass properties in the last two decades in the South Adriatic Sea with emphasis on the period 2006–2009. Continental Shelf Research. doi:10:1016/J.csr.2011.03.002.

Carniel, S., Sclavo, M., Kantha, L.H., Prandke, H., 2008. Double-diffusive layers in the Adriatic Sea. Geophysical Research Letters 35, L02605. doi:10.1029/2007GL032389.

Carniel, et al., 2010. Combining simultaneous seismic reflection and physical oceanographic observations of shelf-slope processes. Geophysical Research Abstracts, EGU General Assembly 12, EGU2010-14267.

Dix, C.H., 1955. Seismic velocities from surface measurements. Geophysics 20, 68–86.

Dorman, C.E., Carniel, S., Cavaleri, L., Sclavo, M., Chiggiato, J., et al., 2006. February 2003 marine atmospheric conditions and the Bora over the Northern Adriatic. Journal of Geophysical Research—Ocean 111 (C03S03). doi:10.1029/2005JC003134.

Geli, L., Cosquer, E., Hobbs, R.W., Klaeschen, D., Papenberg, C., Thomas, Y., Menesguen, C., Hua, B.L., 2009. High resolution seismic imaging of the ocean structure using a small volume airgun source array in the Gulf of Cadiz. Geophysical Research Letters 36, L00D09. doi:10.1029/2009GL040820.

Gonella, J., Michon, D., 1988. Deep internal waves measured by seismic-reflection within the eastern Atlantic water mass. Comptes Rendus de l Academie Des Sciences Serie II 306, 781–787 (in French with English abstract).

Hobbs, R.W., et al., 2007. GO—Geophysical Oceanography: A New Tool to Understand the Thermal Structure and Dynamics of Oceans. D318 Cruise Report. Durham University, Durham, UK. Available from: ⟨http://www.dur.ac.uk/eu.go/cruise/report.html⟩.

Hobbs, R.W., Klaeschen, D., Sallares, V., Vsemirnova, E., Papenberg, C., 2009. Effect of seismic source bandwidth on reflection sections to image water structure. Geophysical Research Letters. doi:10.1029/2009GL040215.

Holbrook, W.S., Pàramo, P., Pearse, S., Schmitt, R.W., 2003. Thermohaline fine structure in an oceanographic front from seismic reflection profiling. Science 301, 821–824.

Holbrook, W.S., Fer, I., 2005. Ocean internal wave spectra inferred from seismic reflection transects. Geophysical Research Letters L15604. doi:10.1029/2005GL023733.

Landrø, M., 1992. Modelling of GI gun signatures. Geophysical Prospecting 40, 721–747. doi:10.1111/J.1365-2478.1992.tb00549.x.

Mirshak, R., Nedimovic, M.R., Greenan, B.J.W., Ruddick, B.R., Louden, K.E., 2010. Coincident reflection images of the Gulf Stream from seismic and hydrographic data. Geophysical Research Letters 37, L05602.

Manca, B.B., Kovacevic, V., Gacic, M., Viezzoli, D., 2002. Dense water formation in the Southern Adriatic Sea and spreading into the Ionian Sea in the period 1997–1999. Journal of Marine Systems 33–34, 133–154.

Nakamura, Y., Noguchi, T., Tsuji, T., Itoh, S., Niino, H., Matsuoka, T., 2006. Simultaneous seismic reflection and physical oceanographic observations of oceanic fine structure in the Kurioshio extension front. Geophysical Research Letters 33, L23605.

Nandi, P., Holbrook, W.S., Pearse, S., Paramo, P., Schmitt, R.W., 2004. Seismic reflection imaging of water mass boundaries in the Norwegian Sea. Geophysical Research Letters 31, L23311.

Papenberg, C., Klaeschen, D., Krahmann, G., Hobbs, R.W., 2010. Ocean temperature and salinità inverted from combined hydrographic and seismic data. Geophysical Research Letters 37, L04601. doi:10.1029/2009GL042115.

Pàramo, P., Holbrook, W.S., 2005. Temperature contrasts in the water column inferred from amplitude-versus offset analysis of acoustic reflections. Geophysical Research Letters 32, L24611.

Polton, J., Hobbs, R., Perratt, O., Vlasenko, V., Inall, M., 2011. Seismic Imaging, Modelling and Observation of the Wyville Thomson Ridge Dense Water Overflow. IUGG Melbourne 2011 P04 122 # 4035.

Ruddick, B., Song, H., Dong, C., Pinheiro, L., 2009. Water column seismic images as maps of temperature gradient. Oceanography 22 (1), 192–205.

Sallarès, V., Biescas, B., Buffett, G., Carbonell, R., Dañobeitia, J.J., Pelegrí, J.L., 2009. Relative contribution of temperature and salinity to ocean acoustic reflectivity. Geophysical Research Letters 36, L00D06. doi:10.1029/2009GL040187.

Sheriff, R.E., 1980. Nomogram for Fresnel zone calculation. Geophysics 45, 968–972.
Sheriff, R.E., Geldart, L.P., 1995. Exploration Seismology2nd Ed. Cambridge University Press.
Taillandier, V., Griffa, A., Poulain, P.-M., Signell, R.P., Chiggiato, J., Carniel, S., 2008. Variational analysis of drifter positions and model outputs for the reconstruction of surface currents in the Central Adriatic during fall 2002. Journal of Geophysical Research—Ocean 113, C04004. doi:10.1029/2007JC004148.
Tsuji, T., Noguchi, T., Niino, H., Matsuoka, T., Nakamura, Y., Tokuyama, H., Kuramoto, S., Bangs, N., 2005. Two-dimensional mapping of fine structures in the Kuroshio Current using seismic reflection data. Geophysical Research Letters 32, L14609. doi:10.1029/2005GL023095.
Turchetto, M., Boldrin, A., Langone, L., Miserocchi, S., Tesi, T., Foglini, F., 2007. Particle transport in the Bari Canyon (Southern Adriatic Sea). Marine Geology 246 (2–4), 231–247.
Vilibic, I., Supic, N., 2005. Dense water generation on a shelf: the case of the Adriatic Sea. Ocean Dynamics 55 (5–6), 403–415.
Wood, W.T., Holbrook, W.S., Sen, M.K., Stoffa, P.L., 2008. Full wave form inversion of reflection seismic data for ocean temperature profiles. Geophysical Research Letters 35, L04608. doi:10.1029/2007GL032359.
Wood, W.T., Lindwall, D.A., Book, J.W., Wesson, J., Carniel, S., Hobbs, R.W., 2011. Seismic Oceanography—A New View of the Ocean, in 2010 NRL Review. Naval Research Laboratory, 4555 Overlook Ave., SW, Washington, DC 20375-5320, pp. 113–121.

REPORT DOCUMENTATION PAGE

Form Approved
OMB No. 0704-0188

1. REPORT DATE *(DD-MM-YYYY)*	2. REPORT TYPE	3. DATES COVERED *(From - To)*
04-12-2012	Journal Article	

4. TITLE AND SUBTITLE

Tracking Bottom Waters in the Southern Adriatic Sea Applying Seismic Oceanography Techniques

5a. CONTRACT NUMBER

5b. GRANT NUMBER

5c. PROGRAM ELEMENT NUMBER

N/A

6. AUTHOR(S)

Sandro Carniel, Andrea Bergamasco, Jeffrey Book, Richard Hobbs, M. Sclavo, Warren Wood

5d. PROJECT NUMBER

5e. TASK NUMBER

5f. WORK UNIT NUMBER

73-9858-A1-5

7. PERFORMING ORGANIZATION NAME(S) AND ADDRESS(ES)

Naval Research Laboratory
Oceanography Division
Stennis Space Center, MS 39529-5004

8. PERFORMING ORGANIZATION REPORT NUMBER

NRL/JA/7330-11-0707

9. SPONSORING/MONITORING AGENCY NAME(S) AND ADDRESS(ES)

Office of Naval Research
One Liberty Center
875 North Randolph Street, Suite 1425
Arlington, VA 22203-1995

10. SPONSOR/MONITOR'S ACRONYM(S)

ONR

11. SPONSOR/MONITOR'S REPORT NUMBER(S)

12. DISTRIBUTION/AVAILABILITY STATEMENT

Approved for public release, distribution is unlimited.

13. SUPPLEMENTARY NOTES

14. ABSTRACT

We present the first results from the seismic oceanography (SO) cruise ADRIASEISMIC where we successfully imaged thermohaline fine structures in the shallow water environment (50–150 m) of the southern Adriatic Sea during March 2009 using a compact two GI-gun seismic source. The SO observations are complemented with traditional oceanographic and micro-structure measurements and show that SO can operate over almost the entire water column except (in our experimental layout) for the uppermost 50 m. After processing to enhance the signal-to-noise ratio, the seismic reflection data have a vertical resolution of ~10 m and a horizontal resolution of ~100 m and provide a laterally continuous map of significant thermohaline boundaries that cannot be achieved with conventional physical oceanography measurements alone. ADRIASEISMIC specifically targeted structures in shallow waters, namely along the western margin of the southern Adriatic Sea, between the Gargano peninsula and the Bari canyon, and imaged the Northern Adriatic Dense Water (NAdDW), a bounded cold and relatively dense water mass flowing from the northern Adriatic Sea.

15. SUBJECT TERMS

seismic oceanography, reflectivity, thermohaline structures, Southern Adriatic Sea

16. SECURITY CLASSIFICATION OF:			17. LIMITATION OF ABSTRACT	18. NUMBER OF PAGES	19a. NAME OF RESPONSIBLE PERSON
a. REPORT	b. ABSTRACT	c. THIS PAGE			Jeffrey W. Book
Unclassified	Unclassified	Unclassified	UU	9	19b. TELEPHONE NUMBER *(Include area code)* 228-688-5251